A review of maser polarization and magnetic fields

W. H. T. Vlemmings[1,2]

[1] Argelander Institute for Astronomy, University of Bonn, Auf dem Hügel 71, 53121 Bonn, Germany

[2] Jodrell Bank Observatory, Univ. of Manchester, Macclesfield, Cheshire SK11 9DL, U.K.
email: Wouter.Vlemmings@manchester.ac.uk

Abstract. Through polarization observations masers are unique probes of the magnetic field in a variety of different astronomical objects, with the different maser species tracing different physical conditions. In recent years maser polarization observations have provided insights in the magnetic field strength and morphology in, among others, the envelopes around evolved stars, Planetary Nebulae (PNe), massive star forming regions and supernova remnants. More recently, maser observations have even been used to determine the magnetic field in megamaser galaxies. This review will present an overview of maser polarization observations and magnetic field determinations of the last several years and discuss the implications of the magnetic field measurements for several important fields of study, such as aspherical PNe creation and massive star formation.

Keywords. masers, polarization, magnetic fields

1. Introduction

Because of their compactness, their high brightness and the fact that they occur in a wide variety of astrophysical environments, masers are excellent astrophysical probes. As the masers are often highly linearly and circularly polarized, polarization observations add fundamental information on both the masing process (such as pumping and level of maser saturation) and the physical conditions in the masing gas. With a detailed theory of maser polarization propagation, the observations can yield the strength of the magnetic field along the maser line of sight and the two-dimensional (or even three-dimensional) field structure. Consequently, they allow for a determination of the dynamical importance of the magnetic field. And, since masers are specifically suited for high angular resolution observations with interferometry instruments, the polarization observations can probe the magnetic field properties at unprecedented small scales.

In the period since the previous IAU maser conference (Migenes & Reid 2002), the number of maser polarization observations have increased significantly. They have been used to determine the strength and structure of magnetic field in the circumstellar envelopes (CSE) of Asymptotic Giant Branch (AGB) stars, high-mass star forming regions and supernova remnants (SNRs), while observations of the magnetic field strength in megamasers have also become possible. This review details specifically the results on magnetic field measurements derived from maser polarization observations since 2001, focusing on the maser transitions in the radio-wavelength regime. In §2, the theoretical background of maser polarization and analysis considerations are discussed briefly. Recent magnetic field measurements and their consequences for related astrophysical problems involving evolved stars and high-mass star forming regions are presented in §3 and §4 respectively. §5 details observations of SNR and megamaser magnetic fields and finally §6 presents perspectives for future instruments and observations.

2. Background and considerations

There exists extensive literature on the theory of maser polarization, as polarization during maser amplification differs from the regular thermal emission case due to the stimulated emission process and a range of other properties of the masing process that can influence the radiation polarization characteristics. The main theoretical problem is framed by constructing the density matrix evolution and radiative transfer equations for the maser emission including the Zeeman terms (Goldreich *et al.* 1973). The Zeeman effect occurs when the degeneracy of magnetic substates is broken under the influence of a magnetic field. The magnitude of the Zeeman effect is significantly different for paramagnetic (e.g. OH) and non-paramagnetic molecules (e.g. SiO, H_2O and methanol), due to the ratio between the Bohr magneton ($\mu_B = e\hbar/2m_e c$) and the nuclear magneton ($\mu_N = e\hbar/2m_n c$). In these expressions e is the electron charge, $\hbar$ is the Planck constant and c the speed of light. The ratio of the two ($\mu_B/\mu_N \approx 10^3$) is determined by the ratio of the electron mass (m_e) and the nucleon mass (m_N) and implies three orders of magnitudes larger Zeeman splitting for a similar magnetic field strength in the case of paramagnetic molecules compared to the non-paramagnetic ones.

A fundamental difference in the treatment of polarized maser emission exists between cases when the magnetic transitions overlap in frequency or when they are well separated. This can be defined by the splitting ratio $r_Z = \Delta\nu_Z/\Delta\nu_D$, where $\Delta\nu_Z$ is the Zeeman splitting and $\Delta\nu_D$ the Doppler line width. Typically, $r_Z \gtrsim 1$ for the paramagnetic molecule OH, while $r_Z < 1$ for the other, non-paramagnetic maser species. In the case of $r_Z > 1$ there are no theoretical ambiguities and the Zeeman components are well separated and resolved. The magnetic transitions $\Delta m_F = \pm 1$ give rise to the $\sigma^{\pm}$ components, circularly polarized perpendicular to the magnetic field B. The transition $\Delta m_F = 0$ gives rise to the π component, linearly polarized along B. For an arbitrary angle between B and the maser propagation direction θ, the resultant components are elliptically polarized for $\theta < \pi/2$, and linearly polarized for $\theta = \pi/2$. The observed splitting of the Zeeman components directly gives the magnetic field strength $B\cos\theta$.

In the case of $r_Z < 1$, the Zeeman components overlap. Theoretical work has been done both analytically and numerically with different implications for the derived magnetic field strengths (e.g.Watson 1994, Elitzur 1996, and references therein). A comparison of the different polarization theories is given by Gray (2003), who finds the numerical models can be used to accurately describe the maser polarization. This is further supported by H_2O maser polarization observations that are best described by the numerical models by Nedoluha & Watson (1992). When $r_Z < 1$ the relation between the linear polarization angle and the magnetic field direction is complex. The magnetic field direction is either parallel or perpendicular to the magnetic field, depending on θ. When $\theta < \theta_{\rm crit} \approx 55°$, the polarization vectors are parallel to the magnetic field and when $\theta > \theta_{\rm crit}$ they are perpendicular. However, this relation is only valid when the Zeeman frequency shift under the influence of the magnetic field $g\Omega$ is much larger than the rate of stimulated emission R. Otherwise, the relation between polarization angle and magnetic field direction is dependent on the maser intensity. However, this is unlikely to affect any except the strongest of maser features. The predicted relation between θ and the polarization angle from H_2O maser theory is supported by the observations of a 90° polarization angle flip when θ crosses the critical angle in combination with the predicted decrease in linear polarization fraction (Vlemmings & Diamond 2006).

The derived B strengths when $r_Z < 1$ do not only depend on the circular polarization fraction but also depend on the maser saturation level. Especially for masers that are saturated, simple assumptions with a fixed proportionality between circular polarization

and magnetic field strength can lead to B being overestimated by up to a factor of 4. On the other hand, velocity gradients along the maser path can cause the true field strength to be underestimated by a factor of two (Vlemmings 2006). Also the blending of maser features in lower angular resolution observations typically causes another factor of two underestimation of B (Sarma et al. 2001).

In both cases ($r_Z < 1$ and $r_Z > 1$) there are several other properties of the maser and its surrounding medium that need to be taken into account when interpreting polarization observations. Especially at the low frequencies, Faraday rotation can make a direct connection between the polarization angle and the B-field uncertain. External Faraday rotation can cause significant vector rotation originating along the line of sight to the maser source. For instance at 1.6 GHz, a typical interstellar electron density and magnetic field strength can cause up to a full $\sim 180°$ rotation towards the W3(OH) star forming region. Additionally, internal Faraday rotation can alter the polarization characteristics of individual maser features in a source in defferent ways, possibly destroying any large scale structure in the linear polarization measurements (e.g. Fish & Reid 2006).

3. Evolved stars and planetary nebulae

Maser polarization observations are the predominant source of information about the role of magnetic fields during the late stages of stellar evolution. Most observations have focused on the masers in the CSEs of AGB stars, as OH, H_2O and SiO masers are fairly common in these sources. However, polarization observations of masers around post-AGB stars and (Proto-)PNe are becoming more common as more such sources with maser emission are found (see Gómez, 2007, these proceedings).

3.1. *AGB stars*

While polarization observations of CSE 1.6 GHz OH masers are fairly commonplace, recent years have seen an increase in 22 GHz H_2O and 43 GHz SiO maser observations of mainly Mira variables and supergiants. As the different maser species typically occur in different regions of the CSE, combining observations of all three species allows us to form a more complete picture of the magnetic field throughout the entire envelope. Close to the central star, SiO maser linear polarization reveals an ordered B-field with a linear polarization fraction ranging from $m_l \sim 15\%$ to $m_l \sim 65\%$ (e.g. Kemball & Diamond 1997). Strikingly, radially elongated jet-like SiO maser structures ,that have been observed around for example o Ceti and R Aql, are apparently aligned with the B-field (Cotton *et al.* 2006). A recent large single dish survey of SiO maser polarization revealed an average field strength of 3.5 G when assuming a regular Zeeman origin of the polarization, indicating a dynamically important B-field (Herpin *et al.* 2006). The observations find no specific support for other (non-Zeeman) interpretations of the polarization.

Further out in the envelope, also 22 GHz H_2O maser measurements reveal significant B-fields, both around Miras and supergiants (Vlemmings *et al.* 2005, and references therein). The measured field strength is typically of the order of $\sim 100-300$ mG but can be up to several Gauss. The strongest field strengths are found around Mira variables, consistent with the H_2O masers occurring closer to the star. As no linear polarization has been detected thus far, describing the magnetic field shape is difficult. However, for the Supergiant VX Sgr, the complex maser structure reveals an ordered field reversal across the maser region consistent with a dipole B-field. Interestingly, the orientation of the field determined from the H_2O maser polarization is similar to the orientation of the
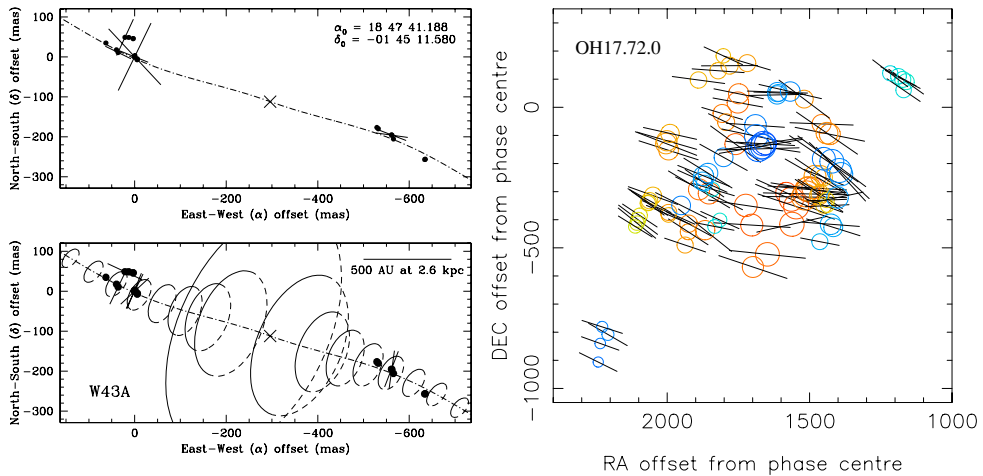
Figure 1. (left; top) The H_2O masers in the precessing jet (dashed-dotted line) of W43A (indicated by the cross). The maser features with the determined linear polarization vectors scaled linearly according to the fractional linear polarization. The polarization vectors lie predominantly along the jet with a median angle of $\chi = 63 \pm 12°$ east of north. (left; bottom) The toroidal B-field of W43A. The vectors indicate the determined direction of B, perpendicular to the polarization vectors, at the location of the H_2O masers. The ellipses indicate the toroidal field along the jet, scaled with $B \propto r^{-1}$ (Vlemmings *et al.* 2006a). (right) The spatial distribution of the 1612 MHz linearly polarized maser components around the P-PNe OH17.7-2.0. Symbol size is proportional to Stokes I flux density; vector size is proportional to logarithmically scaled linearly polarized flux density. More blue-shifted components are represented by darker (blue) symbols and more red-shifted are lighter (red). The clear, overall regular magnetic field structure is consistent with a stretched dipole field (Bains *et al.* 2004)

outflow determined from other H_2O maser observations as well as the orientation of a dipole field determine from OH maser polarization (Vlemmings et al. 2005).

Finally, at typically even larger distances, 1.6 GHz OH maser polarization are fairly common. Often strongly linearly polarized, the masers reveal an ordered B-field at several thousands AU from the star. The field strength at these distances is typically of the order of a few mG (e.g. Deacon *et al.* 2007, in prep.; Etoka & Diamond 2004).

3.2. *Proto-Planetary nebulae*

Most of the polarization work of P-PNe is done on OH masers. Similar to the magnetic field strengths around their progenitor stars, the P-PNe fields are ~ 1 mG in the OH maser region. Single dish surveys reveal linear and circular polarization in respectively $\sim 50\%$ and $\sim 75\%$ of the sources, dependent on the OH maser line (polarization is more common in the 1612 MHz OH satellite line than in the 1665 and 1667 main line masers). The polarization fraction is typically less than 15% (Szymczak & Gérard 2004). The OH maser polarization has also been mapped using MERLIN. As shown in Fig. 1(right), the linear polarization vectors reveal a highly ordered B-field (Bains *et al.* 2003 & 2004).

A very small fraction of the Post-AGB/P-PNe maser stars show highly collimated H_2O maser jets (see Imai 2007; these proceedings). These so-called water-fountain sources are likely the progenitors of bipolar PNe and there are indications that they evolve from fairly high-mass AGB stars. The archetype of this class is W43A (Imai et al. 2002) and polarization observations have recently revealed that the maser jet is magnetically collimated (Fig.1 and 2; Vlemmings et al. 2006a). This lends strong support to the theories of magnetic shaping of PNe (e.g. García-Segura et al. 2005). In addition to the
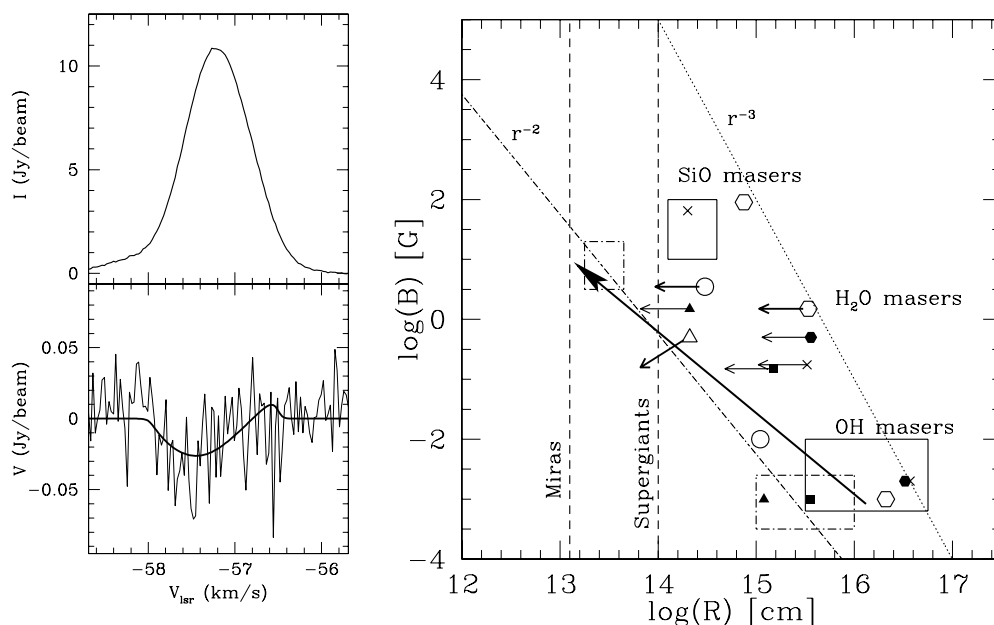
Figure 2. (left) The total intensity and circular polarization spectrum of the H_2O maser feature of W43A for which circular polarization was detected corresponding to a magnetic field strength of 85 mG (Vlemmings et al. 2006a). (right) The figure reproduced from Vlemmings et al. (2005) of measured B-fields on the masers in the CSEs of evolved stars. The dashed-dotted boxes indicate the range of magnetic field strengths measured on the SiO and OH masers of Mira stars and the solid boxes those of Supergiant stars. The thin arrow indicate the H_2O maser B-fields measured in Vlemmings et al. (2002) and Vlemmings et al. (2005), where the length of the arrows indicate the thickness of the H_2O maser shell with the symbols drawn on the outer edge. The symbols without arrows are the measurements on SiO and OH masers from the literature on the same sample of stars. The thick solid arrow indicates B in the jet of W43A.

observations of W43A, recent Australia Telescope Compact Array (ATCA) observations of the likely water-fountain source IRAS 15445-5449 (Vlemmings & Chapman 2007, in prep.) also indicate a magnetic H_2O maser jet.

3.3. *Planetary Nebulae*

There are only a handful of PNe known which show maser emission, and even less of these have masers that are strong enough to provide B-field measurements from polarization observations. One of the sources that shows both OH and H_2O maser emission is the very young PNe K3-35. In this source, the OH masers indicate a B-field of a few mG at 800 AU from the central object (Gómez et al. 2006).

3.4. *Summary*

Fig. 2(right) gives a summary of the current magnetic field measurements in CSEs of both Mira and supergiants. Although the exact relation between the magnetic field strength and distance to the central star remains uncertain, the field strengths are obvious strong enough to dynamically influence the shaping of the outflow and help shape asymmetric PNe. This is further supported by recent observations of strong B-fields on the surface of the central stars in several PNe (Jordan *et al.* 2005) as well as recent PNe dust polarization observations (e.g. Sabin et al. 2007). The magnetic field could also the missing component in the stellar mass-loss mechanism, as recent models indicate the pulsation
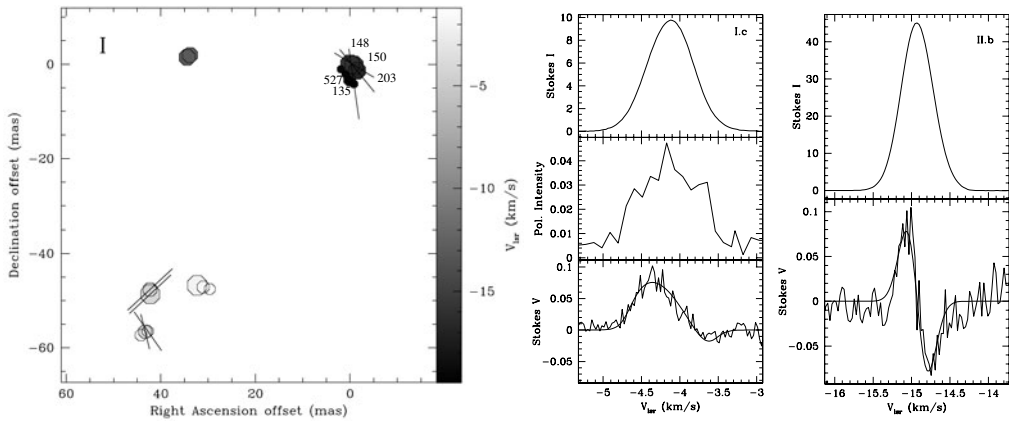
Figure 3. From Vlemmings et al. (2006a): (left) The polarization of the H_2O masers that are argued to be excited in a expanding shockwave through a rotated protostellar disk in Cepheus A HW2 (Gallimore *et al.* 2003). The linear polarization vectors, scaled logarithmically according to polarization fraction P_l, are over-plotted. For the maser features where the Zeeman splitting was detected the magnetic field strength is indicated in mG. (right) Total power (I) and V-spectra for selected maser features in Cepheus A. Additionally, the linear polarized flux density, $\sqrt{(Q^2 + U^2)}$, is shown when detected. The flux densities are given in Jy beam^{-1}. The thick solid line in the bottom panel shows the best non-LTE model fit to the circular polarization V. The V-spectrum is adjusted by removing a scaled down version of the total power spectrum and are clearly not necessarily symmetric.

and radiation pressure alone might not be enough (Woitke 2006). However, the question of the origin of the magnetic field remains and will likely have to be sought in the interaction with a heavy planet, a binary companion or a circumstellar disk, although several models also claim a magnetic dynamo can be maintained by a single star.

4. High-mass star formation

Star forming regions, and especially those forming high-mass stars, often contain a wide variety of maser species tracing many different density and temperature regimes. As was the case for evolved stars, most information on the small scale magnetic fields comes from maser polarization observations, dominated by OH maser measurements but also with an increasing number of H_2O and methanol maser observations. As SiO masers are uncommon during star formation, polarization observations are understandably rare, however, observations of the 86 GHz SiO masers near the massive protostar Orion IRc2 reveal a high level of fractional polarization and a magnetic field along the disk (Plambeck *et al.* 2003).

4.1. *OH masers*

There exists a large number of OH maser polarization measurements, probing densities from $\sim 10^5 - 10^8$ cm^{-3}. OH masers are often strongly polarized and as the Zeeman splitting is large, observations of the separate σ^+ and σ^- components directly yields a magnetic field strength. Observations of the 100% linearly polarized π-component are extremely rare however, likely due to magnetic beaming and the overlap of several differently polarized masers along the line of sight (Fish & Reid 2006). The measured field strengths are typically around ~ 1 mG although recent observation have also revealed individual maser spots with field strengths up to ~ 40 mG (Fish & Reid 2007). The

field direction observed from OH masers seems to maintain the direction of the ambient B-field as the observations show a uniform direction of the field with at most one reversal across regions as large as several arcmin (e.g. Bartkiewicz *et al.* 2005). While linear polarization measurements can sometimes be used to constrain the three-dimensional B-field configuration (e.g. Hutawarakorn *et al.* 2002, Gray et al. 2003), internal and external Faraday rotation make a direct interpretation of the 1.6 GHz OH maser linear polarization difficult.

Magnetic field measurements have also been made using several of the excited OH maser transitions at 6 and 13 GHz. These observations suffer less from Faraday rotation while tracing mostly the same regions of the star forming region. The polarization and B-field values are fully consistent with the lower excitation measurements (e.g. Baudry & Diamond 98, Caswell 2003, Desmurs *et al.* 1998, Etoka *et al.* 2005).

4.2. H_2O masers

After the first discovery of interstellar H_2O maser Zeeman splitting by Fiebig & Güsten (1989) using single dish observations, there have been an increasing number of higher spatial resolution circular polarization observations confirming the earlier results (e.g. Sarma *et al.* 2001, 2002). These observations typically reveal B-field strengths between 15 and 150 mG at densities of $n_{H_2} = 10^8 - 10^{11}$ cm^{-3}. The largest field was recently found in a proposed protostellar disk around one of the several protostars in the Cepheus A HW2 region, with a field strength of ~ 650 mG, as shown in Fig. 3 (Vlemmings et al. 2006b). Such high B-field strength implies a nearby source enhancing the magnetic field. Considering the size of the disk this implies a B-field strength of ~ 2.5 G near the embedded protostar. Alternatively, the observations indicate much higher densities then current H_2O maser theory allows in the shockwave where the masers are excited (Elitzur et al. 1989, and references therein).

In addition to the circular polarization, low levels of linear polarization (typically $\lesssim 2\%$) are also observed in star forming regions. While often structure in the B-field direction is detected, the observations show rapid changes of direction over small scales (see Fig. 3).

4.3. *Methanol masers*

Although the 6.7 and 12 GHz methanol masers are some of the most abundant masers in high-mass star forming regions, polarization observations have been rare. Ellingsen (2002) presented ATCA linear polarization measurements of the 6.7 GHz masers, with a typical polarization fraction $m_l \sim 1.5\%$, while Koo *et al.* (1988) presented similar polarization fractions for the 12.2 GHz maser. Finally, Wiesemeyer *et al.* (2004) claim up to 40% linear polarization of the millimeter methanol masers. Only recently has the first 6.7 GHz methanol maser polarization map been made of the star forming region W3(OH), as shown in Fig. 4(left) (Vlemmings et al. 2006c). These observations show that the B-field is aligned with the large scale methanol maser filament and are consistent with previous OH maser observations. Importantly, the observations show that because they are less influenced by both internal and external Faraday rotation, methanol masers are better probes of the overall B-field structure than OH masers. Since the Zeeman splitting of methanol is small and circular polarization measurements are often hindered by dynamic range problems, the observations of Vlemmings *et al.* (2006c) only provide an upper limit to the B-field strength. However, the first tentative detection of a B-field strength from methanol observations has recently been made (Green *et al.* 2007, this proceedings).
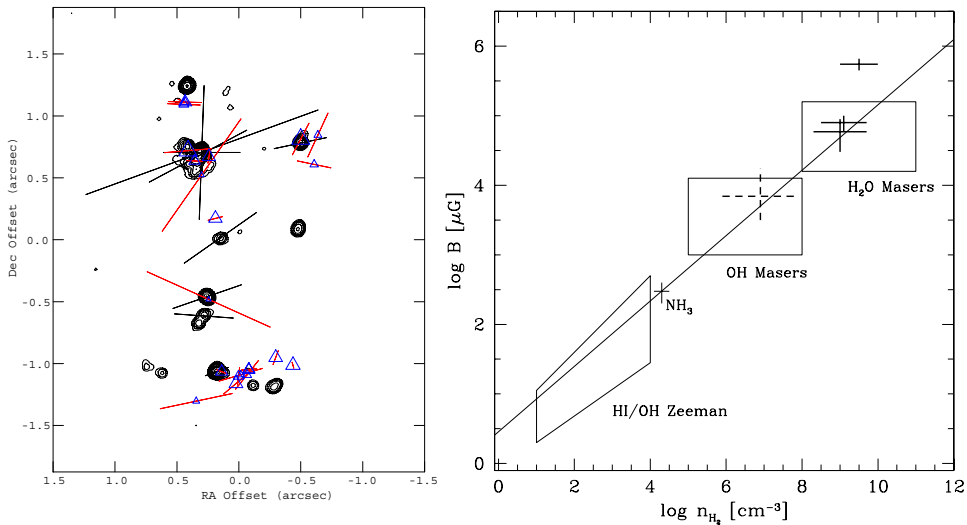
Figure 4. (left) The methanol masers of W3(OH) (contours) including the polarization vectors (black) scaled linearly according the fractional linear polarization (Vlemmings et al. 2006c). The positions in the map are indicated with respect to R.A.(J200)= $02^h 27^m 03.7743^s$, Dec(J2000)= $61°52'24.549''$. The (blue) triangles denote the main line OH masers from Wright et al. 2004b for which polarized intensity was detected at 5σ significance (polarized flux > 75 mJy), and the grey (red) vectors are their linearly scaled polarization vectors. The main line OH maser polarization vectors lengths are scaled down by a factor of 5 with respect to the lengths of the methanol maser polarization vectors. (right) The magnetic field strength B in massive star forming regions measured from Zeeman measurements as a function of n_{H_2}, the number density of neutral hydrogen. The boxes indicate the literature values for HI/non-masing OH, OH maser and H_2O maser Zeeman splitting observations. Also indicated are the H_2O maser measurements (thick solid crosses) and OH maser measurements (thick dashed cross) in the star forming region Cepheus A (Vlemmings *et al.* 2006b, Bartkiewicz et al. 2005) as well as an NH_3 measurement for the same source from Garay et al. (1996). The solid line is the empirical relation $B \propto n^{0.49}$ determined by Crutcher (1999) fixed to the NH_3 magnetic field measurement.

4.4. *Summary*

Fig. 4 (right) shows the B-field measurements of both masers and non-maser observations as a function of number density. The figure seems to indicate that (with the exception of regions such as the above mentioned protostellar disk), the B-field follows the density scaling law over an enormous range of densities, implying that the magnetic field remains partly coupled to the gas up to the highest number density (see Crutcher 2007, these proceedings). However, the shock excited H_2O masers are short-lived (with a typical lifetime $\tau_m \sim 10^8$ s) compared to the typical adiabatic diffusion timescale at the highest densities ($\tau_d \sim 10^9$ s), implying that in the non-masing gas of similar densities, magnetic field strengths are likely lower due to the adiabatic diffusion. Still, the maser B measurements strongly imply a dynamical importance of magnetic fields during the high-mass star formation process, especially in shaping outflows and jets.

5. Other sites of maser emission

Besides the evolved stars and star forming regions, masers are found in several other types of sources. Of those, both supernova remnant (SNR) masers and megamasers have had polarization measurements reported in the last few years.

5.1. *Supernova remnants*

The 1720 MHz OH masers in SNRs have been the target of several polarization observations and recently high resolution observations have for the first time directly resolved the Zeeman splitting between right- and left-circularly polarized spectra (Hoffman et al. 2005, and references therein). Linear polarization reveals the post-SNR shock B-field is well ordered and consistent with other magnetic field tracers and typical derived B-field strengths are $|B| \sim 0.5 - 1.0$ mG (see Brogan 2007, these proceedings).

5.2. *Extragalactic megamasers*

Finally, both H_2O and OH megamasers have been targeted for polarization studies. As the accretion disk H_2O masers are weak, only upper limits have been determined for the magnetic field strength in the masing region. A limit of 30 mG was found in the disk of NGC 4258, which has been used to determine a black hole accretion rate $< 10^{-3.7}$ M./yr (Modjaz *et al.* 2005). The tightest limit found to date is ~ 11 mG in the disk of NGC 3079 at 0.64 pc from the central black hole (Vlemmings et al. 2007), while a further limit of ~ 150 mG was found for the B-field in the Circinus H_2O maser disk (McCallum *et al.* 2007).

The first actual measurements of surprisingly strong extragalactic maser magnetic field strengths were recently made by Robishaw et al. (2007, these proceedings) on the 1667 MHz OH masers in a number of ultra-luminous infrared galaxies (ULIRGs).

6. Future perspectives

Since the previous IAU maser conference (Migenes & Reid 2002) there has been a huge increase in maser polarization measurements. H_2O maser polarization observations have become much more common, the first extragalactic maser polarization detections have been made and methanol maser polarization observations have shown their enormous potential. With the advent of new instruments such as the SMA and ALMA, high resolution dust polarization observations will soon be able to bridge the gap between the small scale maser magnetic field measurements and the very large scale single dish dust polarization observations. This should finally be able to convincingly show the importance of maser polarization observations in star forming regions for magnetic field studies, where especially methanol masers will be able to play a hugely important role. Further in the future, the SKA should be able to bring H_2O maser observations to a new level, fully imaging the polarization of the H_2O envelopes of evolved stars, PNe and even AGN accretion disks. But already in the near future, existing and soon to be upgraded instruments such as (e)MERLIN, the (e)VLA and the VLBA will be able to answer the questions about the role of magnetic fields during star formation and late stellar evolution by further increasing the size of the source samples.

References

Bains, I., Gledhill, T. M., Yates, J. A., & Richards, A. M. S. 2003, *MNRAS*, 338, 287
Bains, I., Richards, A. M. S., Gledhill, T. M., & Yates, J. A. 2004, *MNRAS*, 354, 529
Bartkiewicz, A., Szymczak, M., Cohen, R. J., & Richards, A. M. S. 2005, *MNRAS*, 361, 623
Baudry A., & Diamond, P. J. 1998, *A&A*, 331, 697
Caswell, J. L. 2003, *MNRAS*, 341, 551
Cotton, W. D., *et al.* 2006, *A&A*, 456, 339
Crutcher, R. M. 1999, *ApJ*, 520, 706
Desmurs, J. F., Baudry, A., Wilson, T. L., Cohen, R. J., & Tofani, G., 1998, *A&A*, 334, 1085

Elitzur, M., Hollenbach, D. J., & McKee, C. F. 1989, *ApJ*, 346, 983

Elitzur, M. 1996, *ApJ*, 457, 415

Ellingsen, S. P. 2002, IAU Symposium, 206, 151

Etoka, S., Cohen, R. J., & Gray, M. D., 2005, *MNRAS*, 360, 1162

Etoka, S. & Diamond, P. 2004, *MNRAS*, 348, 34

Fiebig, D. & Güsten, R. 1989, *A&A*, 214, 333

Fish, V. L., & Reid, M. J. 2006, *ApJS*, 164, 99

Fish, V. L., & Reid, M. J. 2007, *ApJ*, 656, 952

Gallimore, J. F., Cool, R. J., Thornley, M. D., & McMullin, J. 2003, *ApJ*, 586, 306

García-Segura, G., López, J. A., & Franco, J. 2005, *ApJ*, 618, 919

Garay, G., Ramirez, S., Rodriguez, L. F., Curiel, S., & Torrelles, J. M. 1996, *ApJ*, 459, 193

Goldreich, P., Keeley, D. A., & Kwan, J. Y. 1973, *ApJ*, 179, 111

Gómez, Y., Tafoya, D., Anglada, G., Franco-Hernandez, R., Torrelles, J. M., & Miranda, L. F. 2006, *Rev. Mexicana AyA*, 26, 22

Gray, M. D. 2003, *MNRAS*, 343, L33

Gray, M. D., Hutawarakorn, B., & Cohen, R. J. 2003, *MNRAS*, 343, 1067

Herpin, F., Baudry, A., Thum, C., Morris, D., & Wiesemeyer, H. 2006, *A&A*, 450, 667

Hoffman, I. M., Goss, W. M., Brogan, C. L., & Claussen, M. J. 2005, *ApJ*, 627, 803

Hutawarakorn, B., Cohen, R. J., & Brebner, G. C. 2002, *MNRAS*, 330, 349

Imai, H., Obara, K., Diamond, P. J., Omodaka, T., & Sasao, T. 2002, *Nature*, 417, 829

Kemball, A. J. & Diamond, P. J. 1997, *Ap. Lett.*, 481, L111

Koo, B.-C., Williams, D. R. D., Heiles, C., & Backer, D. C. 1988, *ApJ*, 326, 931

Migenes, V., & Reid, M. J. 2002, IAU Symposium, 206

McCallum, J. N., Ellingsen, S. P., & Lovell, J. E. J. 2007, *MNRAS*, 103

Modjaz, M., Moran, J. M., Kondratko, P. T., & Greenhill, L. J. 2005, *ApJ*, 626, 104

Nedoluha, G. E. & Watson, W. D. 1992, *ApJ*, 384, 185 (NW92)

Plambeck, R.L., Wright, M. C. H., & Rao, R. 2003, *ApJ*, 594, 911

Sabin, L., Zijlstra, A. A., & Greaves, J. S. 2007, *MNRAS*, 376, 378

Sarma, A. P., Troland, T. H., Crutcher, R. M., & Roberts, D. A. 2002, *ApJ*, 580, 928

Sarma, A. P., Troland, T. H., & Romney, J. D. 2001, *ApJ*, 554, L217

Szymczak, M., & Gérard, E. 2004, *A&A*, 423, 209

Vlemmings, W. H. T. 2006, *A&A*, 445, 1031

Vlemmings, W. H. T., Bignall, H.E., & Diamond, P. J. 2007, *ApJ*, 656, 198

Vlemmings, W. H. T., & Diamond, P. J. 2006, *ApJ*, 648, L59

Vlemmings, W. H. T., Diamond, P. J., & Imai, H. 2006a, *Nature*, 440, 58

Vlemmings, W. H. T., Diamond, P. J., & van Langevelde, H. J. 2002, *A&A*, 394, 589

Vlemmings, W. H. T., Diamond, P. J., van Langevelde, H. J., & Torrelles, J.M. 2006b, *A&A*, 448, 597

Vlemmings, W. H. T., Harvey-Smith, L., & Cohen, R. J. 2006c, *MNRAS*, 371, L26

Vlemmings, W. H. T., van Langevelde, H. J., & Diamond, P. J. 2005, *A&A*, 434, 1029

Watson, W. D. 1994, *ApJ*, 424, L37

Wiesemeyer, H., Thum, C., & Walmsley, C. M. 2004, *A&A*, 428, 479

Woitke, P. 2006, *A&A*, 460, L9

Wright, M. M., Gray, M. D., & Diamond, P. J., 2004, *MNRAS*, 350, 1272